Available online at www.sciencedirect.com
SCIENCE DIRECT
Synthetic Metals 155 (2005) 352–356
SYNTHETIC METALS
www.elsevier.com/locate/synmet

Carbon-skinned metallic wires and magnetic nanocrystals prepared from metal acetylides

Ken Judai [a], Junichi Nishijo [a], Chie Okabe [a], Osamu Ohishi [a], Hiroshi Sawa [b], Nobuyuki Nishi [a,*]

[a] *Institute for Molecular Science, Nishigo-naka 38, Myodaiji, Okazaki 444-8585, Japan*
[b] *The Institute of Materials Structure Science, 1-1 Ohno, Tsukuba, Ibaraki 305-0841, Japan*

Received 4 January 2005; accepted 8 January 2005
Available online 4 November 2005

Abstract

Cobalt acetylide (CoC_2) is synthesized by ion exchange reaction of CaC_2 with $CoCl_2$ in acetonitrile under oxygen and water-free condition. CoC_2 produces carbon-skinned nano-metallic crystals. Inclusion of 20% $SmCl_2$ provides the particles with a larger cohesive force. Cu_2C_2 synthesized by a reported method with some modifications produces nanowires with diameters 5–20 nm. Excitation of these nano-objects by electron beam or ArF laser, or simple heating produces carbon-skinned metallic nanowires and nanocrystals stable in air.

Keywords: Metal–semiconductor magnetic heterostructures; Scanning transmission electron microscopy; Magnetic measurements; Phase-segregated composite interfaces

1. Introduction

Transition metal acetylides (MC_2: M = Ti, Mn, Fe, Co, Ni, and Cu) have been believed to be unstable and easily decomposed even by water [1]. In fact, the acetylides with metal cations lighter than Fe^{2+} are very reactive with water. We have reported that water and oxygen free conditions allow us to obtain cubic nanocrystals of CoC_2 and the structure of the nanocrystals changes to tetragonal upon the exposure to air by inclusion of water molecules [2–4]. Water insertion elongates a_1 and a_2 axes from 4.82 Å to 5.37 Å but shorten a_3 axis from 4.82 Å to 3.40 Å, exhibiting ferromagnetic properties of $(CoC_2)_2(H_2O)$. Water insertion to NiC_2 is not so easy and the full hydration of a few nm crystal in the air is expected to take several days. Once they are prepared, CoC_2 and NiC_2 are stable even for the washing with water.

The magnetic and electronic properties of the acetylide compounds are related to geometrical configuration of metal atoms surrounded by C_2^{2-} dianions. Hsu et al. reported the electrochemical production of Sn, Pb, or Bi nanowires with carbon tube walls [5]. The optical excitation with VUV laser beams, electron beam irradiation and simple heating of the MC_2 or M'_2C_2 compounds are expected to induce segregation into the metal core and the carbon mantle because of the absolute stability of the neutral species [6]. Fig. 1 shows the schematic representation of segregation process by electron transfer from C_2^{2-} anion to M^{2+} cation. Optical or electron beam excitation of an electron in a π^* orbital of C_2^{2-} to charge-transfer states exhibits large transition probability due to the direct electron movement in the electromagnetic field of photons or the field induced by the inelastic electron collision. Such charge-transfer excited states or ion-pair states are characteristic of electron donor–acceptor complex systems [7]. The extreme limit of the charge-transfer state is an ion-pair state, D^+–A^-, and this state exists in most of molecules and complex systems, normally with an energy much lower than the ionization potential of each molecule or that of electron donor species. A metal acetylide molecule is expected to show an electronic nature of charge localized ground state [8]. This nature is enhanced for clustering. In the bulk solid, such a salt sate is not the most stable state. High temperature annealing tends to put the salt into the mixtures of neutral pure elements. Explosive chain reaction of solid Ag_2C_2 or Cu_2C_2

* Corresponding author. Tel.: +81 564 55 7350; fax: +81 564 54 2254.
E-mail address: nishi@ims.ac.jp (N. Nishi).

0379-6779/$ – see front matter © 2005 Elsevier B.V. All rights reserved.
doi:10.1016/j.synthmet.2005.09.012

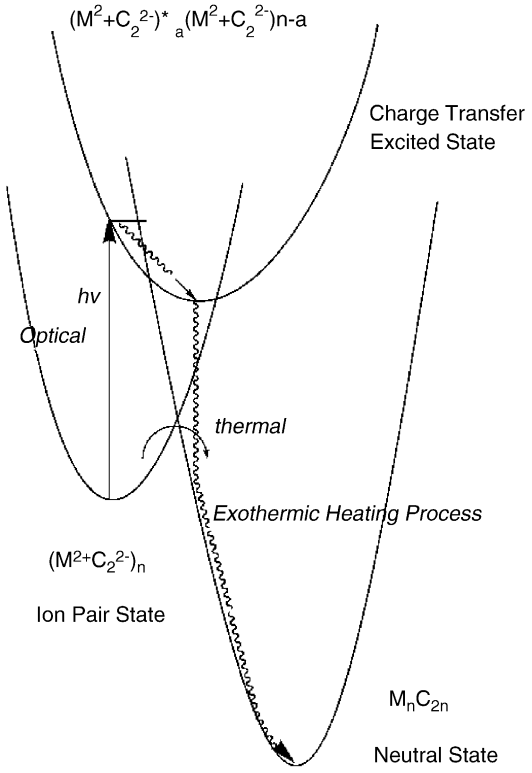

Fig. 1. Scheme of charge neutralization in M_nC_{2n}.

even in Ar atmosphere can be due to very large exothermic energy produced by the back charge-transfer process.

2. Experiments

2.1. Synthesis

Fine particles of CaC_2 (3 mmol) were suspended in 300 mL of acetonitrile solution of $CoCl_2$ (3 mmol) and heated in a 500 mL Pyrex tube situated in a pressure-resistant stainless vessel at 100 °C for CoC_2 over 24 h on oxygen and water-free conditions. Carbon-encapsulated Co–Sm nanomagnets were synthesized in a similar way to that of CoC_2. $CoCl_2$ and $SmCl_2$ were mixed in a ratio of 4:1 with fine particles of CaC_2 (5 mmol) and the reaction temperature in acetonitrile atmosphere was kept at 240 °C for 24 h. As a reference, carbon-encapsulated Co nanocrystals were synthesized under the same condition without $SmCl_2$. Cu_2C_2 was synthesized by flowing Ar with 5% C_2H_2 into 100 mL of aqueous ammonia solution (5%) with 10 mmol of CuCl at room temperature [9]. Flow rate was controlled at a 10 sccm. Produced reddish black solids were suspended in methanol by a supersonic cleaning bath.

2.2. Measurements

The upper part of the suspension was used for microscope observations by a cold field emission scanning electron microscope (SEM), JSM6700F and a high resolution analytical transmission electron microscope (TEM), JEM-3100FEF UHR (JEM-3200).

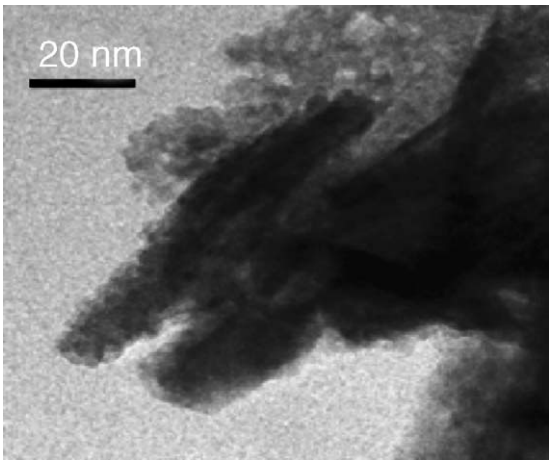

Fig. 2. TEM image of hydrated CoC_2 rods and particles.

X-ray diffraction (XRD) patterns of the nanoparticles were measured with *Mac science* MXP^3VA powder X-ray diffractometer at 293 K, using Cu Kα radiation (λ = 1.5418 Å). Magnetic susceptibilities were measured by using *Quantum-Design* MPMS-XL SQUID magnetometer for powder sample embedded in epoxy resin to keep CoC_2 nanoparticles from rotating.

3. Results

3.1. Room-temperature molecule-based magnet $(CoC_2)_2(H_2O)$

The presence of C_2^{2-} and Co^{2+} is confirmed with the observation of the C=C molecular stretching doublet band at 1422 cm^{-1} and 1475 cm^{-1} in the infrared absorption spectrum and the spectral feature of X-ray absorption near edge structure, respectively. Fig. 2 shows a transmission electron microscope image of hydrated CoC_2 rods and particles, where the rods with diameters of approximately 10 nm and lengths of 40–150 nm are seen as well as the tiny particles with diameters approximately 5 nm. The latter small particles are 80–90% in abundance and highly dependent on the heating condition. Only the 10–20% are composed of rod-type crystals that exhibit magnetic hysteresis at room temperature. Fig. 3 shows the magnetic hysteresis curve of the hydrated sample synthesized at 100 °C. Approximately

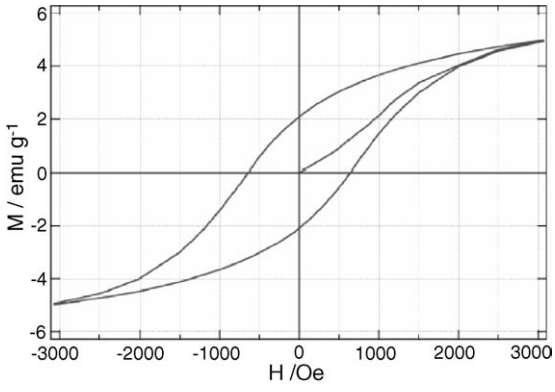

Fig. 3. Magnetic hysteresis curve of the CoC_2 synthesized at 100 °C.

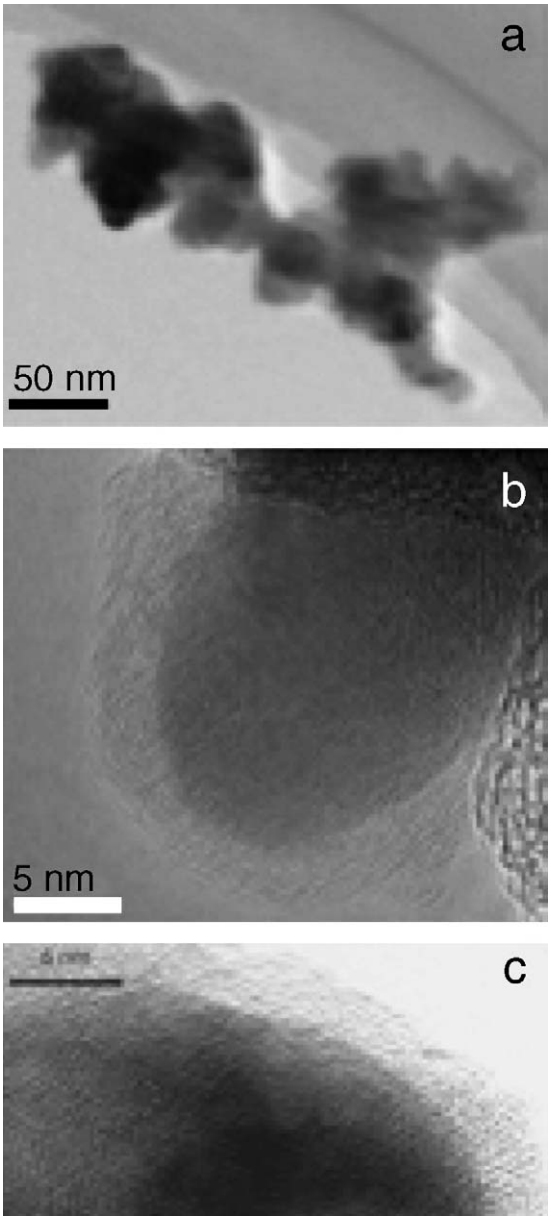

Fig. 4. TEM images of the three kinds of particles produced from $CoCl_2$–$SmCl_2$ (4:1) mixtures. (a) Cohesive particles. (b) A fcc cobalt particle. (c) A hexagonal closed-packed cobalt particle.

10% of CoC_2 units are joined together to form rod-like crystals that behave as room-temperature magnets. This abundance was estimated on the basis of the saturation magnetizations at 1.8 K and 300 K. The saturation magnetization of the CoC_2 particles at 1.8 K was 67 emu g^{-1} that is just expected for a ferromagnetic system with $S = 1/2$. The magnetic hysteresis curves exhibit that the cohesive force is 780 Oe at 1.8 K and 650 Oe at 300 K. These large values are attributed to the enhancement of the anisotropy in the rod-like CoC_2 crystals (Fig. 2).

3.2. Carbon-skinned Co and Co–Sm nanomagnets

The X-ray diffraction pattern of the products from $CoCl_2$–$SmCl_2$ (4:1 mixture) showed broad peaks at $d = 1.95$ Å and 2.05 Å corresponding to the two types of Co crystals, hexagonal close-packed and cubic close-packed structures in addition to a broad but strong new peak at 1.99 Å. The abundance of the hexagonal Co particles is higher than that of cubic one. Note that the segregation reaction of NiC_2 exclusively produces hexagonal closed-packed Ni, although the normal Ni particles produced from other methods show cubic closed-packed structure. It is interesting that the use of the acetylides for the carbon-skinned Co and Ni produces unique structural species dependent on the atomic species. Fig. 4 shows some TEM images of carbon-skinned Co nanocrystals from $CoCl_2$–$SmCl_2$ (4:1) mixtures. However, most of the particles are carbon-skinned Co crystals and Sm seems to be located between the cobalt crystals making the particles cohesive as seen in Fig. 4(a). As seen in the top image, the particles tend to stick together. It is too hard to isolate each particle on a grid disk. From the lattice patterns of the images, one can also confirm the production of the cubic closed-packed Co particles. The magnetic hysteresis curves of the products produced from the 4:1 mixture is shown on the left side of Fig. 5. On the right side the hysteresis curves obtained for the products produced without $SmCl_2$. Apparently, the cohesive forces are very much enhanced in the mixture system. The mixture system exhibits the cohesive forces of 850 Oe and 560 Oe at 1.8 K and 300 K, respectively, while those seen in the pure Co system are 605 Oe and 290 Oe at 1.8 K and 300 K, respectively. The isolation of pure Co–Sm alloy particles is highly desired for the characterization.

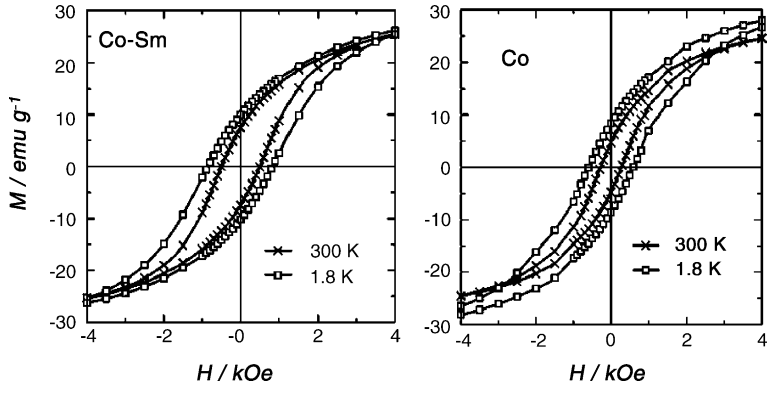

Fig. 5. Magnetic hysteresis curves of the particles produced from $CoCl_2$ and $SmCl_2$ (4:1 mixture) (left) and pure carbon-skinned Co particles (right).

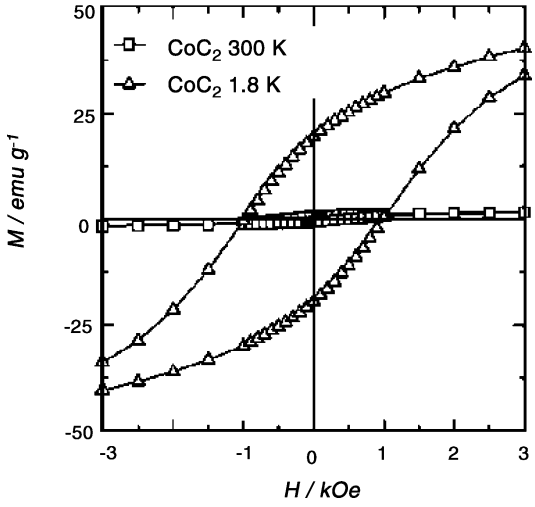

Fig. 6. Magnetic hysteresis curves of CoC_2 particles synthesized at 78 °C.

We can see that the cohesive forces of pure Co and Co–Sm metallic particles are relatively smaller than those of CoC_2 acetylide compounds. As shown in Fig. 6, the cohesive force of CoC_2 amounts to 1000 Oe at 1.8 K. Although the amount of the room-temperature magnet component varies with synthesis temperature and the size of the crystalline domain, it exhibits a cohesive force of 650 Oe at 300 K twice as high as that of the metallic Co particles.

3.3. Generation of carbon-encapsulated Co nanoparticles by VUV laser irradiation on a CoC_2 disk

ArF laser irradiation at 193 nm on a CoC_2 disk produces spherical particles of Co encapsulated in amorphous carbon mantle. Fig. 7 shows a SEM image of carbon-encapsulated Co particles deposited on a Si(1 1 1) plate. These particles were generated by laser sputtering of a CoC_2 disk situated 4 cm in front of the Si plate. Although the particles with the size of 100–150 nm can be seen clearly, most of the particles exhibit the size distribution of 40–60 nm that is a little bit larger than that seen in the Co particles described in the previous section. The white image of

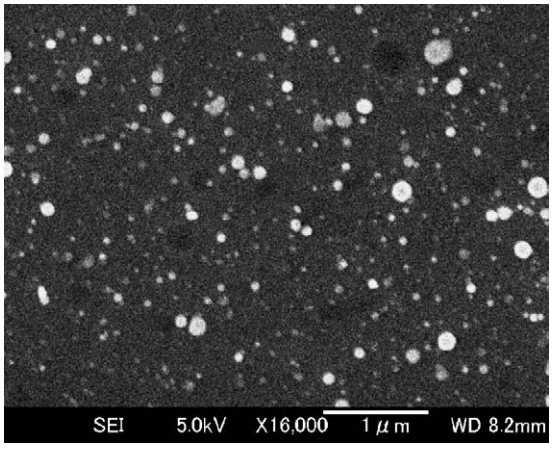

Fig. 7. SEM image of carbon-encapsulated Co particles produced by ArF laser irradiation of a CoC_2 disk.

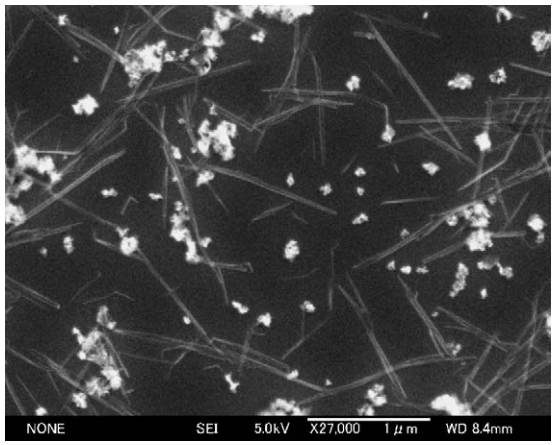

Fig. 8. SEM image of Cu_2C_2 wires. Tiny white particles are amorphous Cu_2C_2.

the particles is due to the charge-up on the surface of the carbon mantles.

3.4. Carbon-encapsulated Cu metal wires from Cu_2C_2

The synthesis of Cu_2C_2 is somehow risky because of its explosive character [9]. However, the control of the acetylene flow rate enabled us to make wire-shaped crystals with a size of 5–6 nm as a single wire. Normally, we get them as bundles of the wires. Fig. 8 shows a SEM image of the Cu_2C_2 solids. As seen in the image, non-wire amorphous solids are also produced while the relative yield of the both solids is controllable. The length of the wires is dependent on the synthetic condition. Careful control of the reaction rate allows us to obtain the wires longer than 1 μm, while normally it varies from 100 nm to 1 μm. X-ray diffraction spectrum exhibited broader peaks and sharper peaks which correspond to the size of the lattice direction. On TEM or SEM measurements, electron beam exposure with high beam density or long time exposure induces the segregation of Cu_2C_2 into metallic wire core and carbon mantle. Fig. 9 shows the TEM image of the segregated wire bundles. In the bandles, black stripes are seen indicating the presence of Cu wire cores with an average radius of 2.5 nm. The inserted image shows the central Cu wire with the carbon mantle. Electron energy loss imaging of Cu and C species clearly demonstrates that the core wire is Cu and the mantle is carbon with distinct π electron systems.

4. Discussion

The diameter of the Cu wire core is approximately 25 Å as is seen in the inserted image of Fig. 9. This diameter means that along the radius direction only 10 Cu atoms are located, Approximately 80 Cu atoms are sit on the circular plane of a typical wire. The Cu atoms on the outer surface (or the interface region) are connected with carbon atoms. Apparently, energy levels of these atoms are shifted from those of the inner Cu atoms. The second layer Cu atoms also show the different energy levels from those of the third layer inner atoms. Thus, only the limited Cu atoms near the center may show Fermi levels responsible to the electric conductivity. On the other hand, the interface 80 Cu

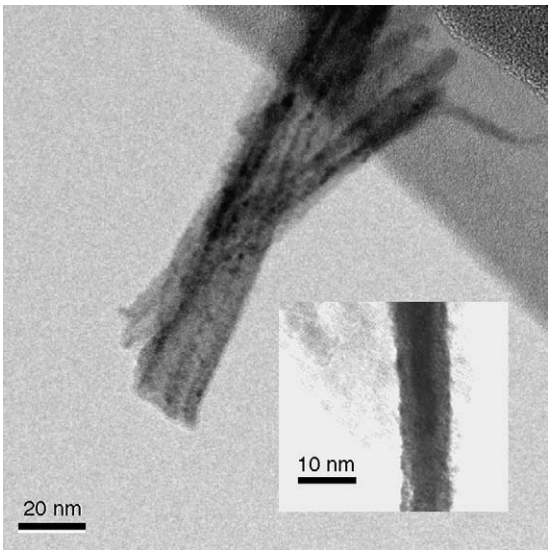

Fig. 9. TEM image of the segregated Cu wire cores in carbon mantles. Inserted is an image of isolated Cu wire with carbon mantle.

atoms are expected to show unique electronic properties if they are connected equivalently along the parallel to the wire direction [10,11]. The annealing procedure is necessary for shaping the central wire crystal. Measurement of position-sensitive electric conductivity of this wire is highly interesting.

The transition metal acetylides can produce various carbon-encapsulated metal nanocrystals. The shape and their properties depend on the electronic properties of metallic species and the way of preparation.

Acknowledgements

This work is supported by a program entitled “Research for the Future of Japan Society of the Promotion of Science” (RFTF: 99P01201). A part of this work is also supported by Grants-in-Aid for Scientific Research (13NP0201) and “Nanotechnology Support Project” of the Ministry of Education, Culture, Sports, Science and Technology (MEXT), Japan.

References

[1] A.F. Wells, Structural Inorganic Chemistry, Clarendon Press, Oxford, UK, 1990 (Chapter 22).
[2] N. Nishi, K. Kosugi, K. Hino, T. Yokoyama, E. Okunishi, Chem. Phys. Lett. 369 (2003) 198.
[3] J. Nishijo, C. Okabe, J. Bushiri, K. Kosugi, N. Nishi, H. Sawa, Eur. Phys. J. D 34 (2004) 217.
[4] N. Nishi, K. Kosugi, K. Hino, T. Yokoyama, Eur. Phys. J. D 24 (2003) 97.
[5] W.K. Hsu, J. Li, H. Terrones, M. Terrones, N. Grobert, Y.Q. Zhu, S. Trasobares, J.P. Hare, C.J. Pickett, H.W. Kroto, D.R.M. Walton, Chem. Phys. Lett. 301 (1999) 159.
[6] K. Kosugi, M.J. Bushiri, N. Nishi, Appl. Phys. Lett. 84 (2004) 1753.
[7] N.J. Turro, Modern Molecular Photochemistry, The Benjamin/Cummings Publishing Co. Inc., California, 1978 (Chapter 5).
[8] K. Judai, J. Nishijo, N. Nishi, unpublished results of the DFT (B3LYP) calculation using Gaussian03 Package for $(Cu_2C_2)_n$ ($n = 1$–4).
[9] F. Cataldo, Polym. Int. 48 (1999) 15.
[10] W. Steinhogl, G. Schindler, G. Steinlesberger, M. Englehardt, Phys. Rev. 66 (2002) 075414.
[11] R. Ral, Phys. Rev. 68 (2003) 115417.